E = efficacy of catalyst used (amount of reactant converted per unit weight of catalyst)
E_R = ratio of efficacies for two catalyst sizes and also = R_R-$(K\alpha/K\alpha_0)$
F, F_i, F_n = fraction of catalyst activity remaining
F_0 = initial catalyst activity
k_0 = kinetic rate constant for fresh catalyst
k_d = kinetic rate constant for deactivated catalyst
K = constant equal to K_0/D_{eff}
K_0 = constant equal to $C_{PFS}/\nu C_{pc}$
$K\alpha_i$ = defined by eq 13
$K\alpha_0$ = the value of $K\alpha_i$ at $\eta = 1.0$
L = catalyst life
n = reaction order
r = reaction rate
R = catalyst radius
R_R = relative radius, normalized to the catalyst which have $\eta = 1$
S_V = space velocity
t = time
T = temperature
V_B = molecular volume
W_c = catalyst weight
Y = fraction of initial carbon remaining after time t (during burnoff)

Subscripts

L = cylindrical pore
s = sphere

Greek Letters

α, α_i = fraction of catalyst poisoned
η = effectiveness factor for a sphere
θ = catalyst porosity
μ = viscosity
ν = stoichiometric coefficient
τ = catalyst tortuosity
ϕ = Thiele modulus

Literature Cited

Allen, D. W.; Gerhard, E. R.; Liken, M. R., Jr. *Br. Chem. Eng. Process Technol.* **1972**, *17*, 605.
Hegedus, L. L.; Summers, J. C. *J. Catal.* **1977**, *48*, 345.
Hill, C. G. "An Introduction to Chemical Engineering Kinetics and Reactor Design", Wiley: New York, 1977; Chapter 12.
Lee, J. W.; Butt, J. B. *Chem. Eng. J.* **1973**, *6*, 111.
Masamune, S.; Smith, J. M. *AIChE J.* **1966**, *12*, 384.
Satterfield, C. N. "Mass Transfer in Heterogeneous Catalysis", M.I.T. Press: Cambridge, Mass., 1970; Chapters 1 and 5.
Smith, J. M. "Chemical Engineering Kinetics", McGraw-Hill: New York, 1970; Chapter 11.
Weisz, P. B.; Goodwin, R. D. *J. Catal.* **1963**, *2*, 397.
Wheeler, A. "Advances in Catalysis", Academic Press: New York, 1951; pp 250–326.

Received for review April 24, 1980
Accepted January 5, 1981

Hydrodynamics and Mass Transfer in Bubble Columns Operating in the Churn-Turbulent Regime

Derk J. Vermeer and Rajamani Krishna*

Koninklijke/Shell-Laboratorium, Amsterdam (Shell Research B.V.) Badhuisweg 3, 1031 CM Amsterdam-N, The Netherlands

The hydrodynamic behavior of a bubble column has been studied at gas velocities at which large, coalesced bubbles and a small bubble dispersion coexist. A 4 m tall, 0.19 m diameter column with nitrogen and turpentine 5 as gas a liquid phases, respectively, was used as the experimental system. A combination of dynamic gas disengagement data and responses to pulse injection of sparingly soluble tracer gases were used in the analysis to obtain information on hydrodynamics and mass transfer. The data show that, for this system, at superficial gas velocities above 0.1 m/s, virtually all the gas is transported as large, fast-rising bubbles, while small bubbles are merely entrained by local liquid circulations which are maintained by the high energy input into the system. The large bubbles have an irregular, continuously changing shape and reach rise velocities up to 1.8 m/s. It appears that after the initial formation period, no significant shedding from or growth of these bubbles occurs. The gas–liquid mass transfer has been found to be unimpaired by the bubble coalescence here. Values for k_La of large bubbles are in line with other data and extrapolations of literature correlations for k_La. However, k_L values for these large bubbles are an order of magnitude larger than that expected from small bubble correlations. This difference is attributed to the violently turbulent state of the interface between large bubbles and liquid.

Introduction

Bubble columns are used as reactors, absorption columns, or strippers in a wide variety of processes (see, for example, the literature surveys of Fair (1967) and Mashelkar (1970)). Most of the published literature data on bubble columns are restricted to superficial gas velocities below about 0.15 m/s, with the majority of these columns operating in the bubbly flow regime. Bubbly flow prevails at gas velocities below 0.06 m/s. While there have been experimental studies of bubble columns operating at gas velocities above 0.15 m/s (Bach, 1977; Hills, 1976; Reith, 1968; Ueyama and Miyauchi, 1977), a clear picture of the hydrodynamics and mass transfer under these conditions is yet to emerge.

The hydrodynamics of a bubble column operating above superficial gas velocities of 0.15 m/s, corresponding to the "churn-turbulent regime" (Bach, 1977), is more complex than that of bubbly flow, and is dependent to some extent on the column diameter. Thus in small diameter columns (less than 0.1 m in diameter) slugging results under these conditions, while in large diameter columns (diameters in excess of 0.15 m), bubble clusters coalesce into large fast-rising bubbles (Bach, 1977; Jekat, 1975). Very little is known about the hydrodynamics of large bubbles coexisting with a dispersion of smaller bubbles. Kölbel et al. (1972) have measured the contribution of large and small bubbles to gas holdup by analyzing frequency distributions in the gas holdup as measured by γ-ray absorption. The investigations were carried out with demineralized water in a 0.092 m diameter column. The smallness of the column diameter would probably suggest that slugging was occurring. The passage frequencies of

0196-4305/81/1120-0475$01.25/0

spontaneous large bubbles (or conceivably slugs) were determined by Ohki and Inoue (1976) in 0.04 and 0.08 m internal diameter columns. For the system air–water, the frequencies were found to lie in the range of 1.5 to 2 s^{-1}. Hills and Darton (1976) measured rise velocities of large bubbles in a dispersion of small bubbles. The high rise velocities determined, of the order of 1 m/s, were attributed to the irregular, ever-changing shape of the large bubbles. Kim et al. (1977), in their study of bubble size and rise velocity in two-phase (gas–liquid) and three-phase fluidized beds, found rise velocities of large bubbles, having diameters of up to 0.08 m, approaching 2 m/s, considerably above the values predicted by the Davies–Taylor relationship for single, isolated bubbles. In addition to these studies, a vast amount of data is available on spherical cap bubbles (e.g., Coppus, 1977). The form of large bubbles in a dispersion of small bubbles is irregular (Hills and Darton, 1976) and the applicability of hydrodynamic and mass transfer data on spherical cap bubbles to practical operating conditions is open to question.

The studies referred to above the deal with different aspects of the problem in isolation. Although such studies are invaluable for the understanding and interpretation of the physical phenomena taking place, they fail to present a design engineer with an integrated approach suitable for scale-up purposes. In the current study, we attempt to provide such an approach for bubble column performance operating at gas velocities up to 0.3 m/s with special attention being given to the churn-turbulent regime of operating. Both hydrodynamics (gas holdup and bubble rise velocities) and mass transfer (k_La) have been studied and an attempt has been made to highlight the close interrelation between them.

Experimental System

The tests were performed in a 4.5 m tall, open-ended Perspex column with an internal diameter of 0.19 m. A flat bottom plate with a cross-shaped sparger was used to create a fine dispersion. The temperature of the column could not be controlled independently; thus small temperature variations took place during the course of the work. As temperatures were mainly between 15 and 20 °C, an average temperature of 17 °C has been used in the data analyses.

A part of the experiments involved measuring gas phase residence time distributions (RTD). Pulse injection of tracer gases was done at the centre of a $^1/_2$-in. nitrogen supply line about 1 m upstream of the sparger. Operation of a three-way solenoid valve by an electronic timer especially suited for small pulse times (typically less than 0.2 s) allowed a fairly smooth tracer flow, this resulting in a 1 to 2% volume tracer concentration in the main gas stream during the pulse. At the outlet of the column a 0.12 m high cone filled with York demister mat was placed as close as possible to the top of the dispersion level. All exiting gas passed through this cone and was exhausted via a 1 m, 0.013 m diameter tube. From this combined gas stream a small, continuous sample stream was analysed by a fast response, microflow catharometer (Taylor Servomex DK 223).

In the reported experiments nitrogen was used as the gas phase and turpentine 5 as the liquid phase. Turpentine 5 is a C_{10}–C_{12} isoparaffin mixture with a 4.5 wt % aromatic content; at 17 °C its physical properties are: ρ = 761 kg/m^3, $\eta = 0.94 \times 10^{-3}$ Ns/m^2, $\gamma = 24.3 \times 10^{-3}$ N/m.

Experimental Data

All experimental data were obtained from liquid dispersion heights of 2 and 4 m, in the absence of liquid flow into or out of the column ("static" liquid pool). Visual observations revealed that at gas velocities above 0.1 m/s coalescence occurred close to the bottom of the column above the gas distributor with the formation of large bubbles; these coalesced large bubbles were irregularly shaped (as also described by Hills and Darton (1976)) and moved rapidly upward through the dispersion of small bubbles. They did not attain the size or shape of slugs, and after initial formation no significant growth occurred as far as could be gauged visually.

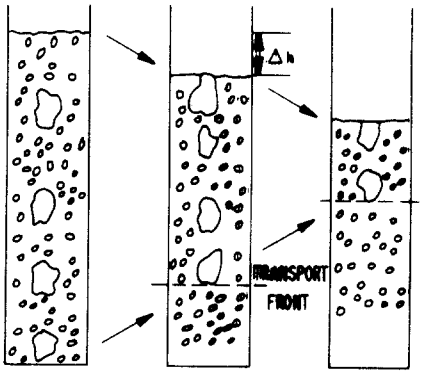

Figure 1. Schematic representation of dynamic gas disengagement process.

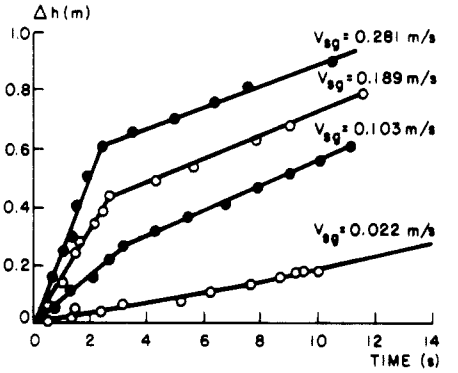

Figure 2. Dynamic gas disengagement process at various superficial gas velocities (column height 4 m).

In addition to visual observations, two other types of experiments were performed in order to analyze the hydrodynamics and mass transfer in sparged columns at gas velocities at which fine dispersion and large bubbles coexist, these being dynamic gas disengagement (DGD) and measurements of responses to pulse injection of tracer gases of varying solubilities.

Dynamic gas disengagement (DGD) occurs when at a certain instant, the gas supply to the column is stopped. The dispersion level will decrease with time while gas continues to escape. Figure 1 depicts schematically the DGD process for a column operating in the churn-turbulent regime. It is assumed that the hydrodynamic condition between the top of the dispersion at the column top and the front of the rising big bubbles does not change in the initial phase of the disengagement process. Typical DGD curves, i.e., level decrease vs. time, are shown in Figure 2; the data points were read from video recordings of the DGD process. The decrease in height is not smooth at high gas velocities, this resulting in some spread in the data points. At low gas velocities, below 0.06 m/s, the dispersion disappears at a uniform rate (bubbly flow regime). Figure 2 shows a typical disengagement in the bubbly flow regime occurring at V_{sg} = 0.022 m/s. The slope of the curve is equal to the superficial gas velocity at the point of disengagement (disengagement starts from bottom upward). At gas velocities above 0.1 m/s, two distinct regions in the DGD curves are discernible. The

Table I. Physical Properties of Tracer Gases

tracer gas	mol fraction of dissolved gas in turpentine 5 at 1 atm pressure[a] 25 °C	17 °C	Henry coeff. at 17 °C	molar volume, cm^3/mol	D_L,[b] $\times 10^{-9}$ m^2/s	$HD_L^{1/2} \times 10^{-5}$ $m\ s^{-1/2}$
helium	0.000228	0.000208	0.0222	4	13	0.253
argon	0.00235	0.00241	0.257	28.5	4	1.63
methane	0.00485	0.00505	0.540	29	4	3.41

[a] Values from Prausnitz (1969); solubility parameter $\delta = 7.5\ (cal/cm^3)^{1/2}$. [b] Diffusion coefficient obtained from Wilke-Chang correlation; using molecular weight of turpentine 5 = 170.

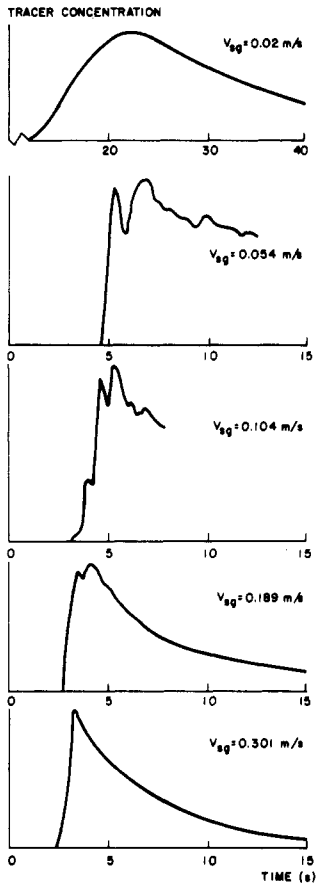

Figure 3. Residence time distribution with helium as tracer; column height 4 m.

first, sharply decreasing part, corresponds to the disengagement of the large bubbles from the system, while the second, slowly decreasing part, corresponds to the disengagement of the entrained small bubbles.

In addition to DGD measurements, dynamic responses to pulse injection of trace gases of various solubilities were obtained. For this purpose He, Ar, CH_4, and to a lesser extent CO_2 were used. The relevant physical properties of these tracer gases are listed in Table I. As may be seen, helium is virtually insoluble in turpentine 5. Figure 3 shows the effect of superficial gas velocity on the RTD of helium. These curves have been taken with special care in order to retain as much resolution as possible. This was achieved by keeping the gap between cone and liquid surface as small as possible and drawing a sample stream at high velocity. At low gas velocities a smooth, somehwat skewed distribution is found, as is typical of axially dispersed flow. A fraction of the gas can be seen to be breaking through rapidly at V_{sg} = 0.054 m/s, even though a long tail still remains. At even higher gas velocities, the bulk of the tracer appears quite rapidly at the outlet and individual large bubbles are discernible in the output as individual peaks (discretized gas flow). As can be seen from Figure 3, individual (bubble) peaks can no longer be

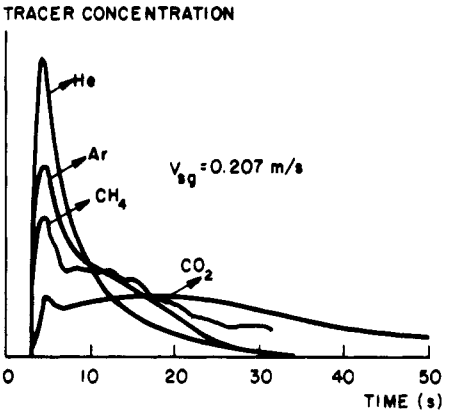

Figure 4. RTD curves with tracer gases of varying solubility; column height 4 m.

distinguished at V_{sg} = 0.30 m/s. This loss in resolution may be due to increased bubble frequency or can be caused by an increase of a few centimeters in the gap space between the dispersion level and the cone demister that was necessary to accomodate sloshing.

Figure 4 shows a typical comparison of the effect of gas solubility on the RTD curve. The initial part of the RTD curve assumes a less distinct peak shape with increasing gas solubility and at the same time decreases in relative size. Also, with increasing solubility a second distribution is developing (see Figure 4) which at first manifests itself as a plateau, as for CH_4 and is fully developed for CO_2.

Data Analysis

The analysis of experimental data will be presented in terms of hydrodynamics and mass transfer. The DGD results are mainly related to hydrodynamics while the mass transfer data are based on analysis of the RTD curves. As will be seen later in the discussion, both sets of data are so interwoven that the subheadings used in this section are for the purposes of presentation only.

Column Hydrodynamics. The DGD curves at higher gas flow rates show two distinct regions (see Figure 2). The first one, corresponding to the sharply decreasing portion, has a slope equal to the superficial gas velocity. The gas leaving the dispersion rapidly has therefore to be considered the instantaneous "transport part" of the total gas holdup, while the gas leaving subsequently (the second slowly disappearing part) has to be viewed as contributing to the gas holdup but not to the net transport of gas at the moment that the transport front is passing. The latter part of the gas holdup is presumably entrained by local liquid circulations which are known to be present (Hills, 1974). The strength of these circulations can be appreciated from the high energy input into the system, e.g., 2.24 kW/m^3 liquid V_{sg} = 0.3 m/s.

The total gas holdup can now be split into two fractions, referred to as the "transport" and "entrained" holdup. The results are presented in Figure 5 and 6 for 4 m and 2 m dispersion heights, respectively. Both "entrained" and "transport" holdups show an increase with increasing gas

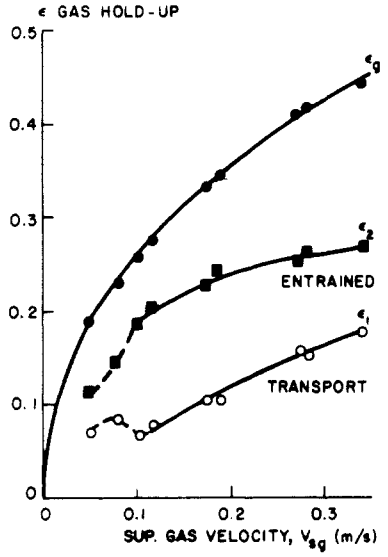

Figure 5. Total gas holdup, transported gas holdup, and entrained gas holdup in column of height 4 m.

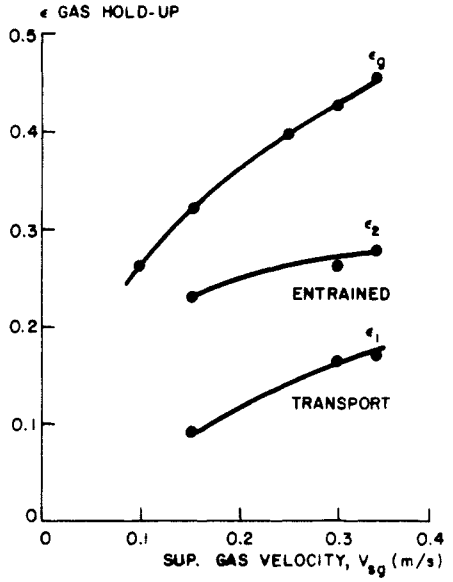

Figure 6. Total gas holdup, transported gas holdup, and entrained gas holdup in column of height 2 m.

velocity at higher gas flows. It is remarkable that the entrained holdup for the experimental system nitrogen–turpentine 5 is considerably larger than the transport holdup. The holdup curves in Figure 5 have a peculiar shape at velocities between 0.05 and 0.1 m/s. This behavior will be better appreciated after further development of the hydrodynamic model.

The rise velocities of the transport front relative to the gas–liquid interface may also be obtained from the DGD curves. This rise velocity should be equal to the average rise velocity during normal operation provided that the assumption of unchanged flow conditions in the initial period of dispersion collapse holds (no additional coalescence). These rise velocities for a 4 m dispersion height are shown as solid points in Figure 7. In addition, residence time distributions such as shown in Figure allow, after corrections for dead time, determination of the rise velocities of bubble-cluster-grown coalesced bubbles. The average rise times of the first discernible peaks in the RTD curves have been used for this purpose and shown in Figure 7 as open points. Figure 7 shows rise velocities approaching 1.8 m/s, considerably larger than those found by Hills and Darton (1976) in an air–water system. The

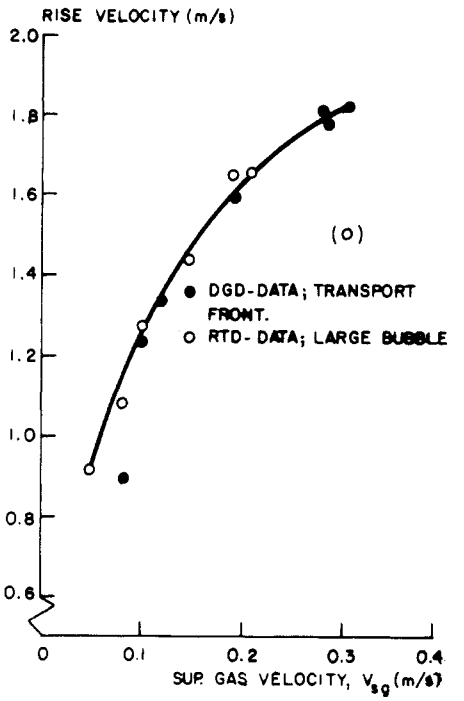

Figure 7. Rise velocities of transport front and individual large bubbles as function of superficial gas velocity.

higher rise velocity observed here for the nitrogen–turpentine 5 system may be due to the increased small bubble (entrained) holdup and/or to the physical properties of the system. More importantly, it should be noted that above a certain superficial gas velocity (about 0.1 m/s), the average rise velocity of the transport front is the same as the rise velocity of the individual large bubbles. The deviation observed in Figure 7 for V_{sg} = 0.3 m/s may be due to loss of resolution in the detection of individual bubble peaks. The conclusion to be drawn at this point is that at gas velocities above 0.1 m/s, the transport part of the gas holdup must consist of large, fast-rising bubbles, possibly with small bubbles in their wakes.

Mass Transfer. Ideally, a mathematical model based on physical reality should be used to extract the relevant mass transfer data from the RTD curves. However, many, as yet unquantified, interactions occur in the system, e.g., the formation process of large bubbles, the axial dispersion of small bubbles in the presence of large bubbles, the net transport of gas by small bubbles, direct small bubble–large bubble interaction, etc.; therefore an attempted fit of the experimental data on the RTD to a multi-parameter axial dispersion type model is likely to lead to a meaningless set of parameter values. A less complicated approach, aimed at obtaining mass transfer rates from large bubbles only, will made below. As will be seen, the results of the simplified analysis are consistent with independently obtained data on column hydrodynamics.

As it was visually determined that the large bubbles followed a spiral path up the column and suffered no backmixing, we assume plug flow for this portion of gas. While some axial dispersion occurs between the top of the liquid and the detector, the major dispersion in the initial phases of the breakthrough curve is due to discretized gas flow, i.e., big bubbles passing at a frequency between 1 and 5 s^{-1} (see Figure 3). A sharp, short duration pulse of an insoluble tracer gas is then expected to appear as a symmetric, slightly broadened distribution at the column outlet if none of the tracer ends up in locally circulation small bubbles. This is, in fact, also clearly brought out in the RTD curves of partially soluble gases such as CH_4 and CO_2

(see Figure 4), where fast and slow-moving parts of the tracer are more separated. The initial part of the CH_4 and CO_2 RTD curves tends to a symmetric distribution. The processes that cause the spread of the leading portion of the RTD (resulting from discretized gas flow) would do the same at the rear side were it not for the mass transfer effects and the small bubble contribution. Even though the evidence is circumstantial at this moment, it appears reasonable to assign the first symmetric distribution in the RTD (i.e., symmetric around the peak of the RTD curve) to the tracer that has been taken immediately by large bubbles without first entering the locally circulating small bubble dispersion.

A simplified mathematical model for obtaining the mass transfer coefficients for the gas moving through the column will now be derived. A fraction f_0 of the total amount of tracer, Q, gets into a bubble cluster(s) that will directly go up the column in plug flow. These tracer-containing bubble(s) have a combined volume V. The initial gas phase concentration of the tracer is then

$$c_0 = f_0 Q/V \tag{1}$$

It is assumed that this bubble cluster, after rapid coalescence, preserves its identity; i.e., no significant shedding or growth occurs after the initial formation period (see below). The material balance may then be written as

$$V\frac{dc}{dt} = -k_L A(Hc - c_L) \tag{2}$$

where c represents the gas phase tracer concentration; c_L is the concentration of the tracer in the liquid phase at the corresponding position; A is the interfacial area of the tracer-containing large bubble; k_L is the liquid phase mass transfer coefficient, and H is the Henry coefficient. Equation 2 implies a liquid phase mass transfer process; this can be verified for the various tracer gases used, all of which have low solubility (See Table I). A fast rising tracer-containing large bubble is in contact with liquid containing no tracer during its rise period and therefore we may set $c_L = 0$ during the initial peiod of the RTD response. With this simplification, we may integrate eq 2 to obtain

$$c = c_0 \exp\left(-k_L \frac{A}{V} Ht\right) \tag{3}$$

By setting $a' = A/V$ = interfacial area per unit volume of gas transported in plug flow, $t = L/V_{rise}$ = contact time of large bubble of rise velocity V_{rise} in a dispersion height L, $c = fQ/V$ = concentration of tracer in bubble, we may combine eq 1, 2, and 3 to give

$$f = f_0 \exp\left(-k_L a' H \frac{L}{V_{rise}}\right) \tag{4}$$

The quantity f represents the fraction of tracer corresponding to the first symmetric distribution in the RTD curve. By definition f_0 should be the same for all tracer gases.

As the gas–liquid interface of large bubbles experiences continuous renewal during the rise, we may apply Danckwerts' surface renewal mass transfer model and therefore

$$k_L = B\, D_L^{1/2} \tag{5}$$

where B is a constant dependent on the hydrodynamics and D_L is the tracer diffusivity in the liquid. Combination of eq 4 and 5 gives

$$\ln f = \ln f_0 - Ba'HD_L^{1/2}\frac{L}{V_{rise}} \tag{6}$$

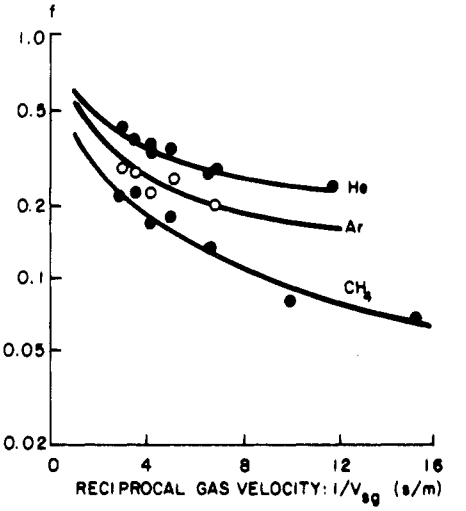

Figure 8. Experimental f values; column height 4 m.

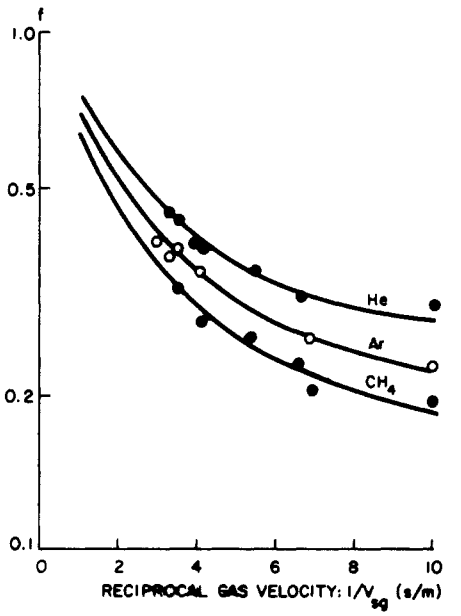

Figure 9. Experimental f values; column height 2 m.

For identical hydrodynamic conditions, the experimentally measured tracer fractions f when plotted as log f vs. $HD_L^{1/2}$ should follow a straight line pattern, as given by eq 6.

For the particular gas–liquid system investigated a large number of RTD curves were obtained for He, Ar, CH_4 tracer gases for both 4 m and 2 m dispersion heights. The fractions f determined from the first symmetric portion of the RTD curve are plotted in Figures 8 and 9 as a function of $1/V_{sg}$. The data points are usually the average of three experiments. The data in Figures 8 and 9 were then smoothed as shown and the smoothed values of f as a function of V_{sg} are plotted in Figure 10 and 11 as log f vs. $HD_L^{1/2}$ at various superficial gas velocities V^0_{sg} (the superficial gas velocity at the column inlet). The physical and transport properties of the various tracer gases used are given in Table I. The superficial gas velocity at the bottom of the column has been used in Figure 10 and 11 to allow comparison of the 4 m and 2 m dispersion data on the basis of equal energy input into the liquid from the entering gas. The observed linearity of the log f vs. $HD_L^{1/2}$ plots suggests the validity of the assumed model for the column hydrodynamics.

The pertinent data obtained from Figures 10 and 11 are given in Table II, together with the calculated results. As may be seen in the table, the f_0 values for the 4 m and 2

Table II. Summary of Experimental and Calculated Results

column height m	V_{sg}, bottom, m/s	V_{sg}, top, m/s	ϵ_g	ϵ_l	ϵ_g/ϵ_l	f_0	L/V_{rise}, s	k_La', s^{-1}	k_La, s^{-1}
4 m	0.10	0.121	0.277	0.080	0.288	0.275	2.97	0.53	0.0424
	0.15	0.180	0.336	0.108	0.322	0.322	2.53	0.55	0.0594
	0.20	0.237	0.382	0.134	0.351	0.360	2.32	0.55	0.0737
	0.25	0.293	0.418	0.158	0.377	0.395	2.20	0.55	0.0866
	0.30	0.349	0.450	0.179	0.397	0.435	2.14	0.56	0.10
2 m	0.10	0.111	0.277	----	----	0.283	1.55	0.47	-----
	0.15	0.165	0.333	0.097	0.292	0.334	1.31	0.49	0.0475
	0.20	0.219	0.375	0.126	0.336	0.384	1.19	0.54	0.0680
	0.25	0.272	0.410	0.150	0.366	0.427	1.12	0.53	0.0795
	0.30	0.325	0.440	0.172	0.391	0.480	1.08	0.55	0.0946

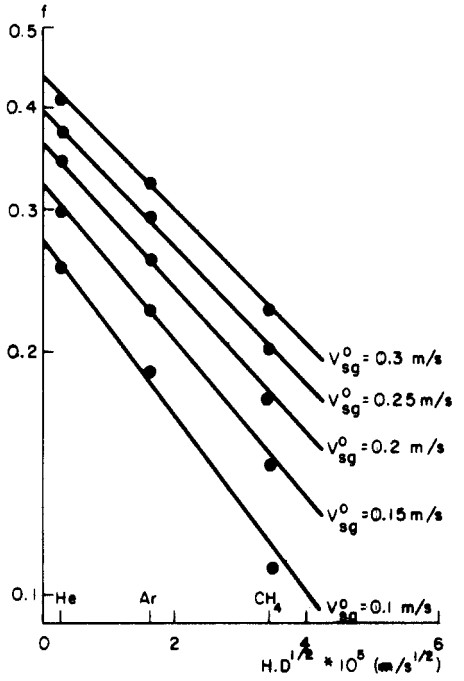

Figure 10. Log f vs. $HD_L^{1/2}$ at various superficial gas velocities (bottom); column height 4 m.

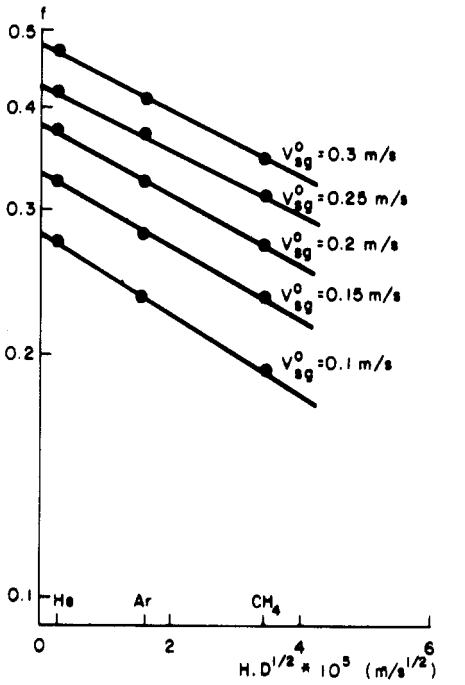

Figure 11. Log f vs. $HD_L^{1/2}$ at various superficial gas velocities (bottom); column height 2 m.

m dispersion heights are approximately equal. The difference found at higher gas velocities is thought to be due to slight interference, at the smaller column height, to the net tracer transport by the axial dispersion of small bubbles with the tracer going up in plug flow. This interference becomes less at the higher column height and at lower gas velocities. Alternatively, it could be argued that slight breakup of large bubbles or bubble clusters travelling in plug flow is resulting in height-dependent f_0 values. For reasons discussed in the next section, this is not considered to be the case.

The slopes of the straight lines in Figures 10 and 11 can be used to calculate k_La', the product of the liquid phase mass transfer coefficient and the interfacial area per unit volume of transported (plug flow) gas. The values of k_La' for transfer of CH_4 in turpentine 5 are given in Table II. It is interesting to note that above V_{sg} = 0.1 m/s, the k_La' values are virtually independent of the gas velocity and column height. The more conventionally used parameter k_La, where a is the interfacial area per unit reactor volume, can be obtained by multiplying k_La' by the transported gas holdup, ϵ_l. These k_La values are given in Table II.

Discussion

In previous sections some important findings from the results have been stressed. Firstly, the rise velocity of the transport front was found to be the same as the rise velocity obtained from the individual bubble peaks in the RTD curves; this is valid at superficial gas velocity above 0.1 m/s. Secondly, the simple mass transfer model was shown to describe the experimental data quite well; these data showed that k_La' is virtually independent of column height and superficial gas velocity above 0.1 m/s. Thirdly, a comparison of f_0 values with the ratios of the transported gas holdup and the total gas holdup, ϵ_l/ϵ_g, (see Table II) shows that these two independently derived values are numerically equal above V_{sg} = 0.1 m/s.

The fraction of the total RTD curve corresponding to the first symmetric distribution for an insoluble tracer gas is f_0, which has been defined as the tracer fraction of the pulse going directly up the column in plug flow. On the other hand, ϵ_l/ϵ_g is the chance that the tracer-containing bubble entering the column at the sparger recombines with the local gas holdup, this containing no tracer, for the net transport of gas. The numerical agreement of f_0 and ϵ_l/ϵ_g suggests that freshly entering small bubbles recombine statistically with bubbles already present, to form bubble clusters which keep their identity while going up the column. Since bubble clusters would certainly break up, it has to be inferred that above a certain critical velocity (i.e., V_{sg} > 0.1 m/s) gas transport occurs exclusively by large, coalesced bubbles. This conclusion is consistent with k_La' being independent of V_{sg}, a result to be expected from discretized gas flow of large bubbles of approximately the same size whose frequency increases with increasing gas velocity. In addition, the correspondence of the rise velocities of the transport front and single, large bubbles also supports the concept that, above V_{sg} = 0.1 m/s, net gas

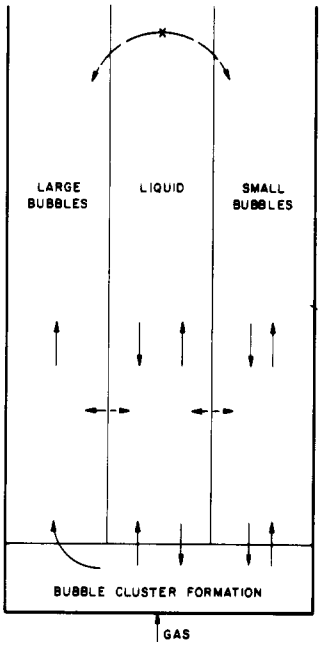

Figure 12. Schematic representation of column hydrodynamics and mass transfer for churn-turbulent regime operation; ↑ flow, ← - → mass transfer; × indicates no interaction between the large and small bubble populations.

transport occurs only by large bubbles which show negligible breakup or growth after the initial formation period.

The conclusions on the column hydrodynamics in the churn-turbulent regime are shown schematically in Figure 12. In the bottom part of the column, incoming gas is finely dispersed by the sparger. At gas velocities above about 0.1 m/s the bubbles regroup, close to the sparger, into bubble clusters, which in the system nitrogen–turpentine 5, coalesce rapidly into large bubbles. Further up the column several simultaneous transport processes occur: transport of gas occurs exclusively by large bubbles; strong liquid circulations cause axial dispersion of small bubble holdup, this resulting in gas of a wide age distribution. Small bubbles might also contribute slightly to the net transport of gas.

Axial dispersion of small bubbles is an important factor in certain column applications and should be an area for further study and modelling. This was considered outside the scope of the present study, but RTD curves, in particular the trailing edge, could yield pertinent information.

Exchange of mass from gas to liquid phase occurs from small and large bubbles, while no direct mass exchange between these two types of bubbles has been shown to exist. In the present study mass transfer from small bubbles (a rather well-known phenomenon) has not been studied; only mass transfer from large, coalesced bubbles has been evaluated here and will now be discussed in somewhat greater detail.

Only a few studies of physical absorption/desorption in bubble columns have been performed at high superficial gas velocities. Towell et al. (1965) have published a few k_L and k_La values for CO_2 desorption from water for V_{sg} between 0.1 m/s and 0.3 m/s. They used a 0.40 m internal diameter column of heights 1.5 and 2.7 m. At higher superficial gas velocities the occurrence of large, coalesced bubbles was reported. Values for k_La were derived from experimental desorption data by assuming plug flow for the gas phase and a completely mixed liquid phase. At V_{sg} = 0.3 m/s, k_La for the system CO_2–H_2O was found to be 0.15 s^{-1}. Mashelkar and Sharma (1970) have corrected Towell's data and a value for k_La of 0.08 s^{-1} is found. Voyer and Miller (1968) measured under similar conditions but in a 0.14 m internal diameter column and obtained a k_La value for CO_2–H_2O of 0.06 s^{-1}. Voyer and Miller (1968) used plug flow for both gas and liquid phases.

At this point in our studies it is not clear whether the results presented here can be directly applied to water as the liquid phase. Even though physical properties and coalescence in the turpentine and water systems are likely to be different, a rough comparison of the data can be made by assuming k_L proportional to $D_L^{1/2}$. Our k_La value for a CH_4–turpentine 5 system, 0.1 s^{-1}, then translates to a value of 0.06 s^{-1} for CO_2–H_2O. This value agrees very well with Voyer's data, which was also obtained in a tall narrow column. It appears though that bubble coalescence to these large irregular-shaped bubbles does not impair the rate of mass transfer. The data at gas velocities above 0.1 m/s form a consistent relationship with the data below 0.1 m/s. In the study reported here we have not covered the low gas velocity range. Use of existing correlations (e.g., Akita and Yoshida, 1974) gives k_La values in line with our reported data for high gas velocities.

Summarizing, the present data and the k_La values reported by Voyer and Miller (1968) are slightly lower than Towell's data as corrected by Mashelkar and Sharma (1970). This difference is not really significant, but according to the hydrodynamic model presented here (gas transported in the form of large bubbles and entrained small bubbles), the column diameter should have an effect on the measured k_La values. In a narrow column, the small bubbles and the liquid phase show less axial dispersion and hence only a small contribution of the small bubbles to the mas transfer. In this context, it is also worth mentioning that Voyer found a rather strong effect of superficial liquid velocity on the derived mass transfer coefficient at higher V_{sg} values. He found that k_La increased while the interfacial area a decreased with increasing liquid velocity. A net cocurrent flow of liquid will cause a net flow of small bubbles which then participate in mass transfer as a parallel stream, while in the absence of cocurrent liquid flow they contribute only slightly through axial dispersion.

Even though are k_La values are in basic agreement with previous data, the present concept of column hydrodynamics leads to much higher k_L values. The data analysis presented here gives k_La values for large bubbles; at V_{sg} = 0.2 m/s and the large bubble frequency is 3 s^{-1} with an associated bubble volume of 0.019 m^3. The interfacial area for the equivalent spherical bubble volume of this size is a' = 40 m^{-1}. Using a k_La' value of 0.5 s^{-1} (see Table II), we obtain k_L = 0.0125 m/s, a value which is about an order of magnitude higher than those predicted from correlations for small bubbles (Calderbank and Moo-young, 1961) or for spherical cap bubbles (Coppus, 1977). The increased k_L value for the large bubbles may be attributed to the violently turbulent state of the gas–liquid interface and to the ever-changing form of these bubbles.

Conclusions

The hydrodynamics and mass transfer of a nitrogen–turpentine 5 system have been studied in a bubble column operating in the churn-turbulent regime, corresponding to superficial gas velocities between 0.1 and 0.3 m/s. It was found that superficial gas velocity V_{sg} > 0.1 m/s rapid bubble coalescence occurs, this resulting in large, irregularly shaped fast-rising bubbles. These bubbles rise at velocities up to 1.8 m/s and transport almost all of the fresh incoming gas up the column. Small bubbles which remain entrained in the column coexist with these large fast-rising bubbles. Use of the dynamic gas disengagement technique allows determination of the large and small

bubble holdups separately. It was found that large bubbles have k_La values which agree with extrapolations of the values in the literature; there is no decrease in these values due to decreased interfacial area a. The k_L values for the large bubbles appear to be an order of magnitude higher than those calculated from correlations derived for small bubbles. It is conjectured that the violently turbulent state of the gas–liquid interface is the cause for this increase.

The data reported here should be applicable to tall, narrow columns in the absence of cocurrent liquit flow. With cocurrent liquid flow a portion of the small bubble population will be transported up the column, giving rise to extra mass transfer.

Our results show that k_La' (= k_La/ϵ_1) is independent of the superficial gas velocity in the range 0.1 and 0.3 m/s. Thus, if one were able to measure, or estimate, the large bubble holdup in the column, the mass transfer coefficient k_La could be easily determined. This suggests a simple scale-up rule for use in practice.

Further experimentation with systems having different physical properties (surface tension, viscosity etc.) will be required to study the factors which determine the bubble size distribution and consequently the gas–liquid mass transfer.

Acknowledgment

The authors would like to express their appreciation to Shell Research B.V. for permitting publication of these results. B. H. Bosman (deceased) and C. N. Garnier performed most of the experimental work reported here and are gratefully acknowledged.

Nomenclature

a = interfacial area per unit volume of reactor, m^{-1}
a' = interfacial area per unit volume of transported gas, m^{-1}
A = interfacial area of tracer-containing gas bubbles going up in plug flow, m^2
B = constant of proportionality used in eq 5, $s^{-1/2}$
c = tracer concentration, mol/m^3
c_0 = tracer concentration at gas inlet, mol/m^3
c_L = tracer concentration in the liquid phase, mol/m^3
D_L = tracer diffusivity in the liquid, m^2/s
f = fraction of RTD curve corresponding to first symmetric distribution
f_0 = value of f at column inlet
H = Henry coefficient
Δh = decrease in height during dynamic gas disengagement, m
k_L = liquid phase mass transfer coefficient, m/s
L = column height, m
Q = quantity of tracer, mol
t = time, s
V = volume of tracer-containing gas (plug flow), m^3
V_{rise} = rise velocity of large bubbles, m/s
V_{sg} = superficial gas velocity (usually at column outlet), m/s
V^0_{sg} = superficial gas velocity at column inlet, m/s

Greek Letters

δ = solubility parameter, $(cal/cm^3)^{1/2}$
ϵ_g = total gas holdup
ϵ_1 = transport gas holdup
ϵ_2 = entrained gas holdup
η = dynamic viscosity, Ns/m^2
ρ = liquid density, kg/m^3
γ = interfacial tension, N/m

Literature Cited

Akita, K.; Yoshida, F. *Ind. Eng. Chem. Process Des. Dev.* **1974**, *13*, 84.
Bach, H. F. Ph.D. Dissertation, Technical University, Munich, 1977.
Calderbank, P. H.; Moo-Young, M. B. *Chem. Eng. Sci.* **1961**, *16*, 39.
Coppus, J. H. C. Ph.D. Dissertation, Technical University, Eindhoven, 1977.
Fair, J. R. *Chem. Eng.* **July 3, 1967**, 67.
Hills, J. H. *Trans. Inst. Chem. Eng.* **1974**, *52*, 1.
Hills, J. H. *Chem. Eng. J.* **1976**, *12*, 89.
Hills, J. H.; Darton, R. C. *Trans. Inst. Chem. Eng.* **1976**, *54*, 258.
Jekat, H. Ph.D. Dissertation, Technical University, Munich, 1975.
Kim, S. D.; Baker, C. G.; Bergougnou, M. A. *Chem. Eng. Sci.* **1977**, *32*, 1299.
Kölbel, H.; Beinhauer, R.; Langemann, H. *Chem. Ing. Tech.* **1972**, *44*, 697.
Mashelkar, R. A. *Brit. Chem. Eng.* **1970**, *15*, 1297.
Mashelkar, R. A.; Sharma, M. M. *Trans. Inst. Chem. Eng.* **1970**, *48*, 162.
Ohki, Y.; Inoue, H. *Chem. Eng. Sci.* **1970**, *25*, 1.
Prausnitz, J. M. "Molecular Theory of Fluid Phase Equilibria", Prentice-Hall: Englewood Cliffs, NJ, 1969.
Reith, T. Ph.D. Dissertation, Technical University, Delft, 1968.
Towell, G. D.; Strand, C. P.; Ackermann, G. H. *A.I.Ch.E. I.Chem.E. symp. Series No. 10*, **1965**.
Ueyama, K.; Miyauchi, T. *Kogaku Kogaku Ronbunshu* **1977**, *3*, 115.
Voyer, R. D.; Miller, A. I. *Can. J. Chem. Eng.* **1968**, *46*, 335.
Wilke, C. R.; Chang, P. C. *AIChE J* **1955**, *1*, 264.

Received for review June 3, 1980
Accepted January 15, 1981

Kinetic Investigation of Wood Pyrolysis

Franz Thurner and Uzi Mann*

Department of Chemical Engineering, Texas Tech University, Lubbock, Texas 79409

The kinetics of wood pyrolysis into gas, tar, and char was investigated in the range of 300 to 400 °C at atmospheric pressure. An experimental system which facilitates the monitoring of the actual sample temperature, collection of gas and tar, and measurement of the sample weight loss as a function of time was developed. It has been found that, in the range investigated, wood decomposition into gas, tar, and char can be described by three parallel first-order reactions as suggested by Shafizadeh and Chin (1977). The activation energies for these reactions are 88.6, 112.7 and 106.5 kJ/mol, respectively, and their frequency factors defined on a mass basis are 8.61×10^5, 2.47×10^8, and 4.43×10^7 min^{-1}. The composition of the pyrolysis products was also analyzed. It was found that the gas consists mainly of carbon dioxide, carbon monoxide, oxygen, and C_3+ compounds with trace amounts of methane, ethylene, and acetylene. The tar consists of seven compounds with levoglucosan accounting for more than half. The char was analyzed by elemental analysis and it was found that its carbon content increases with increasing reactor temperature.

Introduction

The substantial increase in the price of crude oil in the last few years, as well as the concern over the ultimate availability of fossil fuels, prompted increasing interest in using biomass as renewable resources for chemical feedstocks. Wood and other cellulosic materials represent more

0196-4305/81/1120-0482$01.25/0